Biosensors and Bioelectronics 142 (2019) 111574

Contents lists available at ScienceDirect

Biosensors and Bioelectronics

journal homepage: www.elsevier.com/locate/bios

Programming cascaded recycling amplifications for highly sensitive and label-free electrochemical sensing of transcription factors in tumor cells

Xia Li, Jianmei Yang, Ruo Yuan, Yun Xiang*

Key Laboratory of Luminescent and Real-Time Analytical Chemistry, Ministry of Education, School of Chemistry and Chemical Engineering, Southwest University, Chongqing, 400715, PR China

ARTICLE INFO

Keywords:
Transcription factors
Biosensor
Signal amplification
Electrochemical detection

ABSTRACT

The monitoring of transcription factors (TFs) is critical for understanding the regulation of gene transcriptions. Here, by programming nucleic acid sequence-based and cascaded recycling amplifications, we developed a sensitive and non-label electrochemical biosensor for detecting TFs from tumor cell extracts. The binding of the target nuclear factor-kappa B p50 (NF-κB p50) with the dsDNA probes protects them from being digested by exonuclease III for subsequent initiation of three cascaded recycling cycles, which causes the generation of tremendous free G-quadruplex special sequences on the sensing electrode. Such G-quadruplexes can specifically bind and confine hemin within the vicinity of the sensor, generating substantially enhanced reduction current to achieve determination of NF-κB p50 within the range from 0.5 pM to 5 nM with the detection limit down to 0.13 pM. The proposed sensing system also has high selectivity and it can be used to interrogate the presence of NF-κB p50 in tumor cell extracts, demonstrating its potential for disease diagnosis and gene transcription-related studies.

1. Introduction

Transcription factors (TFs) are an important class of regulatory proteins that can regulate gene transcriptions through recognizing the specific sequences of double-stranded DNA (dsDNA) (Potoyan et al., 2017; Zhu et al., 2014). Increasing evidences have revealed that TFs can act as important roles in normal biological functions of gene replications, cell divisions and cell growth, and the dysregulations of signaling TFs were involved in the pathogenic mechanisms of many diseases (Li et al., 2016). For example, the transcription factor, nuclear factor kappa B p50 (NF-κB p50), if aberrantly expressed, is considered to be closely related to asthma, diabetes and cancers (Miyagi et al., 2014; Peng et al., 2016). NF-κB p50 is constitutively active in most tumor cell lines, whether derived from hematopoietic tumors or solid tumors, and is found to be inactive in normal cells, making it a promising biomarker for the evaluation of disease status (Han et al., 1998; Karin, 2006; Serasanambati and Chilakapati, 2016). Therefore, highly sensitive methods for detecting NF-κB p50 are required for the diagnosis of active NF-κB p50-related diseases.

Although many traditional strategies including electrophoresis mobility shift assays (EMSA) (Hellman and Fried, 2007), Western blot (Clarke and Liu, 2010) and enzyme-linked immunosorbent assays (ELISA) (McKay et al., 1998) have been developed for detecting TF binding activities or concentrations, these techniques encounter some limitations. For instance, the EMSA approach requires time-consuming electrophoretic separations and radioactive element labeling that poses a threat to human health and environmental safety. While, the Western blot and ELISA dependent upon the use of antibodies are expensive and involve multistep techniques, limiting their extensive applications. In recent years, a variety of alternative methods, such as electrochemistry (Lu et al., 2017; Peng et al., 2018; Xiong et al., 2016), colorimetry (Rasheed and Lee, 2018; Tan et al., 2010; Zhang et al., 2015), chemiluminescence (Ma et al., 2014; Tonooka et al., 2007) and fluorescence (Ranallo et al., 2015; Zhang et al., 2017; Zhu et al., 2017), have been established for the detection of TFs. Among them, the electrochemistry-based methods have attracted more interests due to their sensitivity, fast response and simple operations. In addition, due to the fact that the expression levels of TFs in biological cells are extremely low, robust amplification strategies are commonly needed for detecting TFs with high sensitivities (Sha et al., 2016).

So far, various amplification strategies including nanomaterials (Melnychuk and Klymchenko, 2018; Yu et al., 2016), strand displacement reaction (Gliddon et al., 2016; Park et al., 2017; Zhang and Winfree, 2009), rolling circle amplification (Zhu et al., 2016), nuclease-assisted recycling (Ma et al., 2017; Shi et al., 2018) and DNAzyme amplification (Fan et al., 2015) have been extensively developed for

* Corresponding author.
E-mail address: yunatswu@swu.edu.cn (Y. Xiang).

https://doi.org/10.1016/j.bios.2019.111574
Received 10 June 2019; Received in revised form 24 July 2019; Accepted 4 August 2019
Available online 06 August 2019
0956-5663/

detecting different biomolecules. Among them, the nuclease-assisted signal amplifications are particularly attractive, owing to their excellent amplification capabilities. For example, exonuclease III (Exo III) can specifically catalyze stepwise digestion of a DNA duplex from the blunt or recessed 3′-end while it has no cleavage function on the single-stranded probe or DNA duplex probe containing the protruded 3′- end (Feng et al., 2018). Because no specific nicking sequence of the DNA probe is required for its function, Exo III is considered to be a promising tool for signal amplification. Therefore, the Exo III-assisted amplification strategy can be used to construct universal biosensing platforms for convenient detection of metal ions, DNA, RNA and DNA-binding proteins (Qu et al., 2017; Xu et al., 2016; Zhang et al., 2019). DNAzyme, an artificial deoxyribozyme, also attracts a lot of attentions because it is a conveniently available synthetic biocatalyst for the construction of amplified sensors. In particular, the metal ion is an essential cofactor for the activation of the specific DNAzyme, and the corresponding substrate sequences for the DNAzyme can be cleaved by the special metal ion to obtain amplified signals (Huang and Liu, 2015; Liu et al., 2017; Wang et al., 2017). Owing to the inherent features of stability, biocompatibility and high catalytic efficiency, DNAzymes have been becoming promising amplification tools for assaying of different biomolecules.

Inspired by the attractive signal magnification capabilities of Exo III-mediated recycles and DNAzymes, we report here an electrochemical biosensor for detecting NF-κB p50 by manipulating multiple and cascaded recycling signal amplifications. The target proteins bind the specific recognition domain of the dsDNA probes and prevent the digestion reaction of the Exo III toward the dsDNA. The protected dsDNA probes hybridize with the assistant hairpin probes to form 3′-blunt ends, and thus Exo III can catalyze stepwise degradation of the assistant hairpin probes, releasing the protein-DNA complex that can again bind hairpin probes and the DNAzyme sequences that hybridize with the corresponding hairpin substrates. Then, Mg^{2+} ions perform the cleavage reactions toward the hairpin substrates, liberating the G-quadruplex segments and other special sequences that hybridize with assistant hairpin probes to activate the successive Exo III-induced cleavages. Such integrated and cascaded recycling amplifications can thus lead to the generation of massive G-quadruplex special sequences on the sensing surface, which can form lots of G-quadruplex/hemin special complexes upon binding to hemin with the assistance of k^+. Therefore, a substantially amplified reduction current can be observed to achieve the determination of the NF-κB p50 target molecules. Our NF-κB p50 sensing method features with two attractive advantages. First, this sensor integrates multiple cyclic signal enhancement reactions to achieve label-free electrochemical detection with low cost and easy manipulation. Second, due to the sequence independence of Exo III, the sensor can be further extended as a universal detection platform to detect other proteins, nucleic acids or enzymes.

2. Experimental section

2.1. Chemicals and reagents

Tris(2-carboxyethyl) phosphine hydrochloride (TCEP), 6-mercapto-1-hexanol (MCH) and the interference proteins including thrombin, bovine serum albumin (BSA) and carcinoembryonic antigen (CEA) were ordered from Sigma (St. Louis, MO). Exo III was supplied by New England Biolabs (Beijing, China). NF-κB p50, HEPES, Tris-HCl, and HPLC-purified oligonucleotides listed below were bought from Sangon Biotechnology Inc. (Shanghai, China). S1: 5′-GAG GGG ACT TTC CCA GGC CGT TTA CAT CTC TTA TTT T-3'; S2: 5′-CCG CCT TGC CTG GGA AAG TCC CCT C-3'; Hairpin probe (HP1): 5′-GTT TAC ATC TCT TCA GCG ATC CGG AAC GGC ACC CAT GTT AGT TAG TTT TTA GAA GAG ATG TAA ACG GGC GG-3'; Hairpin substrate (SH-HP2): 5′-ACC CGC CCG TTT TAC TAA CTA TrAG GAA GAG ATG GGG TAG GGC GGG TTG GGT TTT-$(CH_2)_6$-SH-3' (rA denoted the adenosine ribonucleotide).

The buffers used in this work included the hybridization and immobilization buffer (20 mM Tris-HCl, 5 mM KCl, 10 mM $MgCl_2$, 100 mM NaCl, pH 7.4), DNA-protein binding buffer (10 mM Na_2HPO_4/NaH_2PO_4, 10% glycerol, 10 mM $Mg(CH_3COOH)_2$, 100 mM CH_3COONa, pH 7.4), detection buffer (20 mM HEPES, 200 mM NaCl, 50 mM KCl, pH 8.0) and hemin buffer (20 mM HEPES, 1% DMSO, 200 mM NaCl, 50 mM KCl, pH 8.0).

2.2. Preparation of the sensor

The 3 mm bare gold electrode (AuE) was firstly cleaned for 30 min in the mixed solution of H_2O_2 and H_2SO_4 with 1:3 v/v and rinsed using water. Afterwards, the AuE was sequentially polished by 0.3 and 0.05 μm alumina slurries and was sonicated in water, ethanol and water respectively for 5 min each. Then, the AuE was further cleaned through successive scanning in the solution of H_2SO_4 (0.5 M) within the potential window of -0.3 to 1.55 V. The AuE was finally washed using water again, dried in nitrogen gas flow and used for probe immobilization.

Each hairpin probes (HP1 and SH-HP2) was annealed by heating to 90 °C for 5 min and cooled down to 25 °C with 1 °C min^{-1}. TCEP (10 mM) was then introduced into the SH-HP2 solution to reduce the disulfide. Subsequently, 10 μL of the reduced SH-HP2 (0.3 μM) in immobilization buffer was casted on the AuE surface and further incubated at 25 °C for 2 h. Next, after washing the AuE with immobilization buffer, MCH (1 mM) was added to eliminate the nonspecific DNA adsorption, and the SH-HP2/MCH/AuE was ready for subsequent experiments.

2.3. Amplified NF-κB p50 sensing protocol

The solution of probe S1 and probe S2 in hybridization buffer was heated to 90 °C for 5 min and then slowly (1 °C min^{-1}) cooled down to 25 °C to ensure complete hybridization between probe S1 and probe S2. For the detection of the proteins, the above as prepared S1/S2 (100 nM) was incubated with various concentration of NF-κB p50 in protein binding buffer for 30 min at 37 °C to make protein-DNA binding reaction occur. Subsequently, Exo III (40 U) was introduced and further incubated for 30 min at 37 °C. Next, HP1 (500 nM) was added into this solution and then the resultant mixed solution was interacted with the sensing electrode for 100 min. Followed by rinsing with hemin buffer, the sensor was incubated in hemin buffer containing hemin (0.2 mM) at 25 °C for 30 mim to obtain the desired G-quadruplex/hemin special complexes. This sensor was rinsed with detection buffer and DPV voltammogram was obtained in detection buffer.

2.4. Detection of NF-κB p50 in cell extracts

Hela cells were cultured in DMEM medium with 10% fetal bovine serum (FBS) and 100 U mL^{-1} streptomycin-penicillin in 5% CO_2 incubator at 37 °C. Nuclear extraction of Hela cells was performed by a nuclear extract kit (Active Motif, Carlsbad, CA) and extracted samples were stored at 4 °C for subsequent experiments. Various concentrations of NF-κB p50 were spiked into the diluted nuclear extraction sample (10%) and were detected using the proposed sensor.

2.5. Apparatus

The conventional three-electrode system used in the tests composed of the Ag/AgCl reference electrode, platinum counter electrode and modified AuE working electrode. The electrochemical workstation CHI 852C (Shanghai, China) was utilized to carry out all electrochemical measurements. Cyclic voltammetry (CV) with the scan rate of 50 mV s^{-1} within the potential window of −0.1 to 0.6 V was recorded in KCl (0.1 M) containing $[Fe(CN)_6]^{3-/4-}$ (1 mM). Nitrogen was purged into detection buffer for 30 min to eliminate the interferences

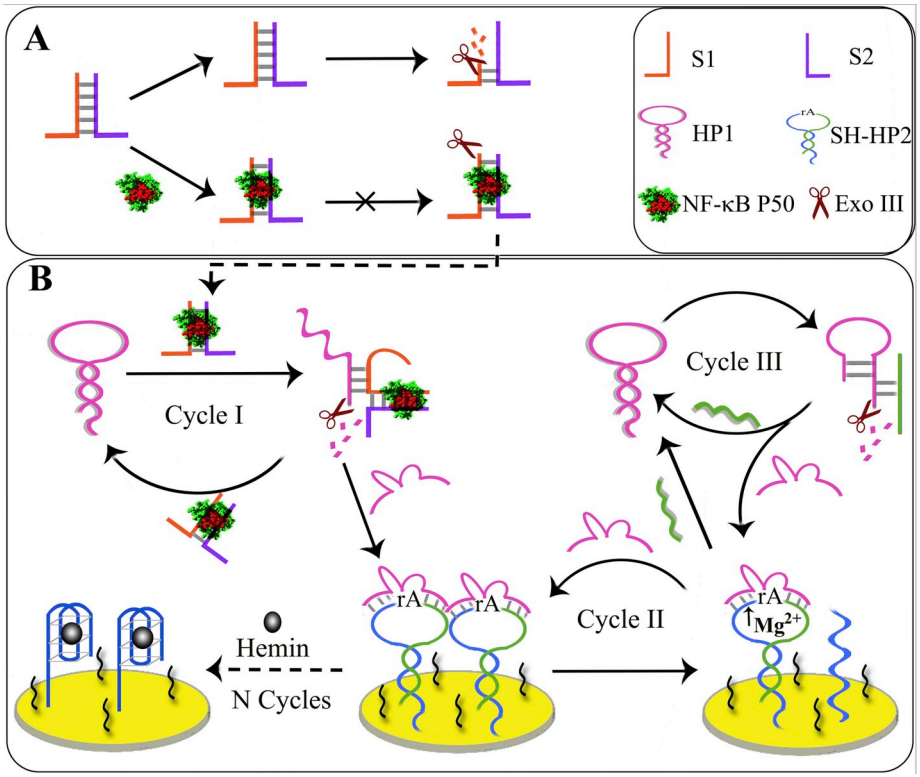

Scheme 1. Electrochemical sensing principle for detecting NF-κB p50 *via* cascaded recycling amplifications.

from the dissolved oxygen before DPV measurements, which were performed from −0.15 to −0.5 V at sampling width of 16.7 ms, pulse width of 25 ms and amplitude of 50 mV.

3. Results and discussion

3.1. Principle of NF-κB p50 sensor

The proposed sensing system, as illustrated in Scheme 1, for detecting NF-κB p50 contains Exo III, double-stranded probes (S1/S2) and two hairpin probes (HP1 and SH-HP2). Exo III that catalyzes stepwise degradation of the S1/S2 duplex DNA probes from the 3′-blunt ends is used to achieve the recycling of the protein-S1/S2 complex in cycle I and to amplify the readout signal in cycle III. The S1/S2 probe has two functional domains: the protein binding domain and the complementary sequence to HP1 that is carefully designed to contain the DNAzyme-caged sequence. The thiol-modified and hairpin-shaped probe (SH-HP2) is consisted of three functional segments: the substrate sequence for the DNAzyme, the G-quadruplex-locked segment and the segment with identical sequence to the free ends of the protein-S1/S2 complex. The S1/S2 duplex can be cleaved by Exo III from the 3′-blunt ends without the participation of the target NF-κB p50. However, with the addition of the protein NF-κB p50, the formed protein-S1/S2 complex via binding specific recognition domain of S1/S2 produce bulky steric hindrance to prevent the digestion of the protein-bound S1/S2 by Exo III. The protected S1/S2 with tails complementary to part of HP1 then hybridizes with HP1 containing 3′-overhang ends to form 3′-blunt ends, and Exo III catalyzes stepwise cleavage of HP1, liberating the protein-S1/S2 complex, which hybridizes with another HP1 to activate the successive Exo III cleavage. Moreover, the released DNAzyme sequences can hybridize with and cleave SH-HP2 assembled on the AuE at the rA sites with the assistance of the Mg^{2+} ions, releasing the G-quadruplex segments and the sequences identical to the free ends of the protein-S1/S2 complex. These sequences can bind HP1 to initiate Exo III cleavage in cycle III. Therefore, the combination of Exo III- and DNAzyme-assisted amplification cascades can thus lead to the production of a great quantity of free G-quadruplex special sequences on the sensing electrode. These sequences can bind hemin to obtain G-quadruplex/hemin special complexes under the assistance of K^+ ions and to confine hemin in the vicinity of the electrode surface, yielding drastically enhanced electrochemical response for sensitively detecting NF-κB p50.

3.2. Characterization of NF-κB p50 sensor

As a powerful technique for characterizing the electrochemical properties of the sensor, CV was performed to verify the sensor fabrication process. As expected, CV of the $[Fe(CN)_6]^{3-/4-}$ probes on unmodified AuE shows two redox peaks (Fig. 1a), testifying the process of electron transfer with fast speed. Because of the electrostatic repulsive force between the negative charges of SH-HP2 and $[Fe(CN)_6]^{3-/4-}$, the current peaks decrease obviously (curve b vs. a) after immobilizing SH-HP2 and MCH on the AuE surface. When the sensor was further incubated with mixed sample of S1, S2, HP1, Exo III and target NF-κB p50, the current peaks increase obviously (curve c vs. b). This mainly because SH-HP2 is cleaved to induce a decrease of the DNA phosphate backbones with negative charges of the sensing surface for the

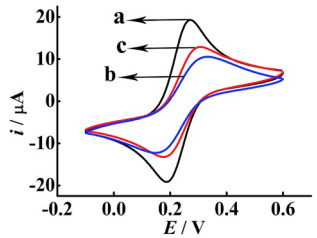

Fig. 1. CV measurements of this developed sensor at various stepwise assembly process: (a) unmodified AuE, (b) SH-HP2/MCH/AuE, (c) (NF-κB p50 + S1 + S2 + HP1 + Exo III)/SH-HP2/MCH/AuE.

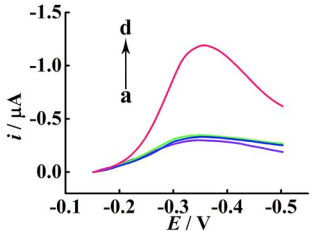

Fig. 2. DPV voltammograms of the AuEs incubated with various mixtures: (a) SH-HP2/MCH/AuE, (b) (HP1 + Exo III)/SH-HP2/MCH/AuE, (c) (S1 + S2 + HP1 + Exo III)/SH-HP2/MCH/AuE, (d) (NF-κB p50 + S1 + S2 + HP1 + Exo III)/SH-HP2/MCH/AuE. Experimental parameters: S1/S2 (100 nM), HP1 (500 nM), SH-HP2 (500 nM), Exo III (50 U), NF-κB p50 (1 nM), hemin (0.2 mM) and the time for Exo III-mediated recycling was 120 min.

reduction of repulsive force.

3.3. Feasibility of NF-κB p50 detection

DPV responses were tested to further demonstrate the feasibility of this proposed sensing system for the target NF-κB p50 detection. We can see an insignificant DPV signal (curve a) of the SH-HP2/MCH/AuE in Fig. 2, possibly because of the non-specifically adsorptive hemin, which indicates the inhibition of the generation of free G-quadruplexes by the hairpin structure. When the reaction mixtures of HP1, Exo III (curve b) and S1, S2, HP1, Exo III (curve c) were separately incubated the sensor electrodes, no obvious increases in DPV peak currents are observed, due to the fact that HP1 cannot be cleaved by Exo III without the participation of NF-κB p50 and subsequent cyclic reactions cannot be completed. However, a significant increase in DPV peak of hemin at about −0.35 V is obtained after the incubation of SH-HP2/MCH/AuE using a mixed solution of S1, S2, HP1, Exo III and NF-κB p50. These above phenomena indicate that Exo III-assisted cleavage reaction of HP1 can occur with the participation of S1, S2 and NF-κB p50, accompanying with the release of the free DNAzyme sequences. The cleavage of SH-HP2 leads to the production of massive free G-quadruplexes and subsequent formation of G-quadruplex/hemin special complexes under the assistance of K^+ ions.

3.4. Optimizations of sensing conditions

Experimental parameters affecting the performance of the sensing system for amplification determination of the NF-κB p50 were further optimized. The response current sharply increases with the concentration of immobilized probe SH-HP2 from 0.1 to 0.3 μM (Fig. 3A) and then decreases beyond 0.3 μM. This phenomenon is caused by the assumption that a low SH-HP2 concentration can reduce the efficiencies while high concentrations might cause steric hindrances for the cleavage of the SH-HP2 and thus relatively decreased signal currents are observed. The concentration of SH-HP2 at 0.3 μM in the following experiments was used. Fig. 3B shows the influence of the Exo III amount on DPV peak current. Obviously, the peak current increases as the Exo III concentration increases from 10 to 40 U while no obvious changes can be obtained when the Exo III amount is beyond 40 U, suggesting that 40 U is the suitable amount for NF-κB p50 determination. Fig. 3C illustrates that the DPV current increases as the reaction time is prolonged and tends to saturation after 100 min. Thus, 100 min was optimal to detect NF-κB p50.

3.5. Sensitivity and selectivity of NF-κB p50 sensor

Under the above selected experimental parameters, we examined the change of DPV current response corresponding to different concentration of target NF-κB p50. Fig. 4A depicts that DPV current

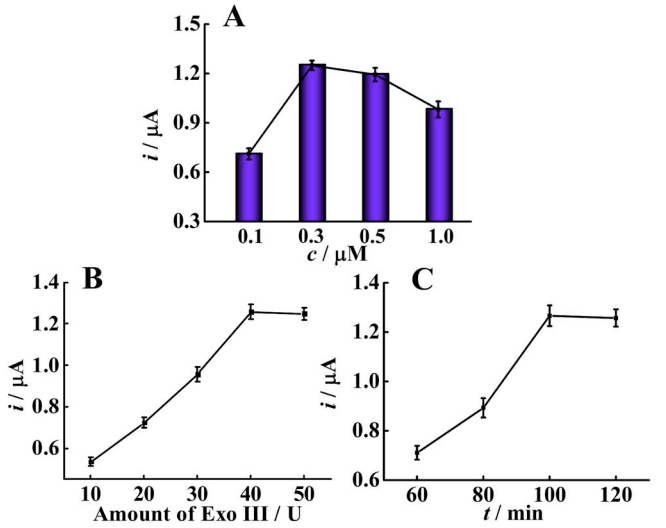

Fig. 3. The effects for (A) the concentration of immobilized probe SH-HP2 and (B) the amount of Exo III and (C) reaction time of Exo III-mediated recycling. The concentrations of S1/S2, HP1, NF-κB p50, hemin were 100 nM, 500 nM, 1 nM, 0.2 mM, respectively. Error bars: SD; n = 3.

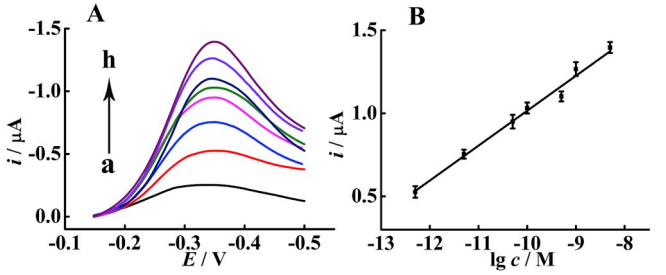

Fig. 4. (A) DPV voltammograms of the sensor for assaying different concentrations of NF-κB p50: (a) 0, (b) 0.5 pM, (c) 5 pM, (d) 50 pM, (e) 100 pM, (f) 500 pM, (g) 1 nM, (h) 5 nM. (B) The resulting calibration plot for DPV current vs. the logarithm of NF-κB p50 concentration. Experimental parameters: S1/S2 (100 nM), HP1 (500 nM), SH-HP2 (300 nM), Exo III (40 U) and time of Exo III-assisted target recycling was 100 min. Error bars: SD; n = 3.

enhances with the incremental concentration of NF-κB p50, and the peak current exhibits a linear relationship with the logarithmic concentration of NF-κB p50 (Fig. 4B). The regression equation is i = 0.21019 log c + 3.1177 from 0.5 pM to 5 nM (i and c represent response current and concentration of NF-κB p50, respectively). The detection limit of this proposed sensor for NF-κB p50 is about 0.13 pM according to the 3σ rule. Such high sensitivity of the sensor, which is basically due to the integration of the Exo III-assisted amplification technique and DNAzyme cleavage signal enhancement, is competitive with previous developed strategies (Table 1). Besides, the measurement of a fixed concentration of NF-κB p50 at 100 pM with six different sensors prepared in the same manner yielded a relative standard deviation (RSD) of 4.6%, demonstrating a good reproducibility of the sensor. Moreover, after the storage of the sensors at 4 °C for three weeks, only 5% decrease in DPV peak current for the concentration of NF-κB p50 at 100 pM is observed, indicating a satisfactory stability of the sensor.

We also examined the selectivity of this sensing system by using different interference proteins of thrombin, BSA and CEA. As evidenced by Fig. 5, small peak currents similar to the background current appear with the addition of the interference proteins (50 nM), whereas a significantly increased signal current is obtained when the NF-κB p50 is added even at a lower (10 folds) concentration (5 nM). These results, as expected, well demonstrate a good selectivity of this electrochemical

Table 1
Comparison assay of various strategies for NF-κB p50 detection.

Method	Amplification strategy	Linear range	Detection limit	Reference
Electrochemiluminesce	ExoIII-aided recycling	0.05 nM-2 nM	17 pM	Xiong et al. (2016)
Colorimetry	nanoparticles	50 pM-1 nM	6.4 pM	Rasheed and Lee (2018)
Fluorescence	ExoIII-aided recycling	50 pM-1 nM	45.6 pM	Du et al. (2019)
Fluorescence	SDA and ERCA	0.38 pM-15 nM	0.2 pM	Zhu et al. (2017)
Electrochemistry	ExoIII-aided recycling	10 pM-5 nM	10 pM	Lu et al. (2017)
Electrochemistry	Exo III and DNAzyme	0.5 pM-5 nM	0.13 pM	this work

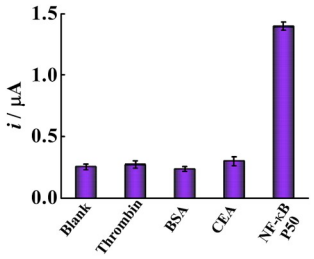

Fig. 5. Selectivity evaluation of the sensor for NF-κB p50 (5 nM) and the interference proteins (50 nM each). Error bars: SD; n = 3.

Table 2
Recovery tests for NF-κB p50 in the diluted nuclear extract of Hela cells (n = 6).

Sample	Added	Found	Recovery (%)	RSD (%)
1	5 pM	4.8 nM	96	3.6
2	50 pM	48.3 pM	96.6	4.5
3	100 pM	105.1 pM	105.1	4.1
4	1 nM	0.98 nM	98	2.3

sensor for NF-κB p50 determination.

3.6. Real samples analysis

The NF-κB p50 assay in diluted nuclear extraction of the Hela cells (10%) was conducted to demonstrate whether this proposed sensing system *via* the integration of Exo III cleavage and DNAzyme-assisted amplification can detect TFs in biological samples. Various concentrations of NF-κB p50 were spiked into 10-fold diluted nuclear extraction samples of Hela cells and the added NF-κB p50 were measured by the sensor. After obtaining the DPV peak currents of the added NF-κB p50, the recovered concentrations were calculated by the regression equation. Table 2 shows that the recovery rate of this sensing system for four different concentrations of added NF-κB p50 ranges from 96% to 105.1% with RSD from 2.3% to 4.5%, which indicates the sensor has the potential to be applied for real samples.

4. Conclusions

To conclude, our study demonstrated a sensitive electrochemical sensing platform for detecting the NF-κB p50 transcription factor on the basis of the integration of DNAzyme- and Exo III-aided cleavage amplification cascades. The presence of the target molecules triggers cascaded recycling cycles to cleave many SH-HP2 containing the G-quadruplex special sequence assembled on the AuE surface, and subsequently the numerous G-quadruplex special sequences are released. These G-quadruplex sequences can bind hemin to generate a substantially amplified current for detecting NF-κB p50 down to 0.13 pM. Importantly, our sensing method has high selectivity for the target NF-κB p50 protein against other interference proteins. Despite the significant signal amplification capability of our approach for transcription factor detection, the involvement of enzymes may potentially cause stability issues, and the multiple operation steps in the assay method are also required as well. Future work on the exploration of enzyme-free and single-step strategy by combining other convenient signal amplifications (e.g., toehold-mediated strand displacement) with DNAzymes for highly sensitive detection of the NF-κB p50 molecules can be envisioned in the near future.

CRediT authorship contribution statement

Xia Li: Conceptualization, Data curation. **Jianmei Yang:** Methodology. **Ruo Yuan:** Formal analysis. **Yun Xiang:** Project administration, Funding acquisition.

Declaration of competing interest

The authors declare that they have no known competing financial interests or personal relationships that could have appeared to influence the work reported in this paper.

Acknowledgment

This work was supported by National Natural Science Foundation of China (No. 21675128) and Fundamental Research Funds for the Central Universities (XDJK2017A001).

References

Clarke, D.C., Liu, X., 2010. Methods Mol. Biol. 647, 357–376.
Du, K.T., Wu, J.Z., Pan, A.Q., Li, D.Y., Cui, L., Peng, C., 2019. Anal. Chim. Acta 1068, 80–86.
Fan, H.H., Zhao, Z.L., Yan, G.B., Zhang, X.B., Yang, C., Meng, H.M., Chen, Z., Hui, L., Tan, W.H., 2015. Angew. Chem. 127 (16), 4883–4887.
Feng, Q., Zhao, X., Guo, Y., Liu, M., Wang, P., 2018. Biosens. Bioelectron. 108, 97–102.
Gliddon, H.D., Howes, P.D., Kaforou, M., Levin, M., Stevens, M.M., 2016. Nanoscale 8 (19), 10087–10095.
Han, Z.N., Boyle, D.L., Manning, A.M., Firestein, G.S., 1998. Autoimmunity 28 (4), 197–208.
Hellman, L.M., Fried, M.G., 2007. Nat. Protoc. 2 (8), 1849–1861.
Huang, P.J.J., Liu, J.W., 2015. Nucleic Acids Res. 43 (12), 6125–6133.
Karin, M., 2006. Nature 441 (7092), 431–436.
Li, K., Wang, L., Xu, X.W., Gao, T., Yan, P., Jiang, W., 2016. RSC Adv. 6 (73), 68846–68851.
Liu, M., Chang, D.G., Li, Y.F., 2017. Acc. Chem. Res. 50 (9), 2273–2283.
Lu, L.H., Su, H.J., Li, F., 2017. Anal. Chem. 89 (16), 8328–8334.
Ma, F., Liu, W.J., Zhang, Q.Y., Zhang, C.Y., 2017. Chem. Commun. 53 (76), 10596–10599.
Ma, F., Yang, Y., Zhang, C.Y., 2014. Anal. Chem. 86 (12), 6006–6011.
McKay, I.A., Kirby, L., Volyanik, E.V., Kumar, V., Wong, P.W., Bustin, S.A., 1998. Anal. Biochem. 265 (1), 28–34.
Melnychuk, N., Klymchenko, A.S., 2018. J. Am. Chem. Soc. 140 (34), 10856–10865.
Miyagi, T., Shiotani, B., Miyoshi, R., Yamamoto, T., Oka, T., Umezawa, K., Ochiya, T., Takano, M., Tahara, H., 2014. Cancer Sci. 105 (7), 870–874.
Park, Y.Y., Lee, C.Y., Park, K.S., Park, H.G., 2017. Chem. Eur J. 23 (68), 17379–17383.
Peng, K.F., Xie, P., Yang, Z.H., Yuan, R., Zhang, K.Q., 2018. Biosens. Bioelectron. 102, 282–287.
Peng, K.F., Zhao, H.W., Xie, P., Hu, S., Yuan, Y.L., Yuan, R., Wu, X.F., 2016. Biosens. Bioelectron. 81, 1–7.
Potoyan, D.A., Bueno, C., Zheng, W.H., Komives, E.A., Wolynes, P.G., 2017. J. Am. Chem. Soc. 139 (51), 18558–18566.
Qu, X.M., Zhu, D., Yao, G.B., Su, S., Chao, J., Liu, H.J., Zuo, X.L., Wang, L.H., Shi, J.Y., Wang, L.H., Huang, W., Pei, H., Fan, C.H., 2017. Angew. Chem. Int. Ed. 56 (7), 1855–1858.
Ranallo, S., Rossetti, M., Plaxco, K.W., Vallée-Bélisle, A., Ricci, F., 2015. Angew. Chem. Int. Ed. 54 (45), 13214–13218.
Rasheed, P.A., Lee, J.S., 2018. Anal. Bioanal. Chem. 410 (4), 1397–1403.

Serasanambati, M.R., Chilakapati, S.R., 2016. South Indian J. Biol. Sci. 2 (4), 368–387.
Sha, L., Zhang, X.J., Wang, G.F., 2016. Biosens. Bioelectron. 82, 85–92.
Shi, C.X., Li, S.X., Chen, Z.P., Liu, Q., Yu, R.Q., 2018. Anal. Chem. 91 (3), 2120–2127.
Tan, Y.N., Su, X.D., Zhu, Y., Lee, J.Y., 2010. ACS Nano 4 (9), 5101–5110.
Tonooka, K., Kabashima, T., Yamasuji, M., Kai, M., 2007. Anal. Biochem. 364 (1), 30–36.
Wang, S., Yue, L., Shpilt, Z., Cecconello, A., Kahn, J.S., Lehn, J.M., Willner, I., 2017. J. Am. Chem. Soc. 139 (28), 9662–9671.
Xiong, Y.W., Lin, L., Zhang, X.J., Wang, G.F., 2016. RSC Adv. 6 (44), 37681–37688.
Xu, M.D., Gao, Z.Q., Wei, Q.H., Chen, G.N., Tang, D.P., 2016. Biosens. Bioelectron. 79, 411–415.
Yu, C.M., Qian, L.H., Ge, J.Y., Fu, J.Q., Yun, P.Y., Yao, S.C., Yao, S.Q., 2016. Angew. Chem. Int. Ed. 55 (32), 9272–9276.
Zhang, D.Y., Winfree, E., 2009. J. Am. Chem. Soc. 131 (47), 17303–17314.
Zhang, H.G., Li, F.Y., Chen, H.L., Ma, Y.H., Qi, S.D., Chen, X.G., Zhou, L., 2015. Sens. Actuators, B 207, 748–755.
Zhang, J.L., Huang, J., He, F.J., 2019. Biosens. Bioelectron. 138, 111322–111329.
Zhang, K., Wang, K., Zhu, X., Xie, M.H., Zhang, X.L., 2017. Biosens. Bioelectron. 87, 299–304.
Zhu, D.S., Wang, L., Xu, X.W., Jiang, W., 2017. Biosens. Bioelectron. 89, 978–983.
Zhu, D.S., Zhu, J., Zhu, Y., Wang, L., Jiang, W., 2014. Chem. Commun. 50 (95), 14987–14990.
Zhu, Y., Wang, H.J., Wang, L., Zhu, J., Jiang, W., 2016. ACS Appl. Mater. Interfaces 8 (4), 2573–2581.